AGU PUBLICATIONS

Geophysical Research Letters

RESEARCH LETTER
10.1002/2014GL061973

Key Points:
- ARTEMIS observes structures that have the properties of collisionless shocks
- Lunar shocks may be driven by solar wind reflection from crustal magnetic fields
- Lunar shocks may represent the smallest collisionless shocks in the solar system

Correspondence to:
J. S. Halekas,
jasper-halekas@uiowa.edu

Citation:
Halekas, J. S., A. R. Poppe, J. P. McFadden, V. Angelopoulos, K.-H. Glassmeier, and D. A. Brain (2014), Evidence for small-scale collisionless shocks at the Moon from ARTEMIS, *Geophys. Res. Lett.*, *41*, doi:10.1002/2014GL061973.

Received 22 SEP 2014
Accepted 16 OCT 2014
Accepted article online 18 OCT 2014

Evidence for small-scale collisionless shocks at the Moon from ARTEMIS

J. S. Halekas[1,3], A. R. Poppe[2,3], J. P. McFadden[2], V. Angelopoulos[4], K.-H. Glassmeier[5], and D. A. Brain[3,6]

[1]Department of Physics and Astronomy, University of Iowa, Iowa City, Iowa, USA, [2]Space Sciences Laboratory, University of California, Berkeley, California, USA, [3]Solar System Exploration Research Virtual Institute, NASA Ames Research Center, Moffett Field, California, USA, [4]Department of Earth, Planetary, and Space Sciences, University of California, Los Angeles, California, USA, [5]Institut für Geophysik und Extraterrestrische Physik, Technische Universität Braunschweig, Braunschweig, Germany, [6]Laboratory for Atmospheric and Space Physics, University of Colorado, Boulder, Colorado, USA

Abstract ARTEMIS observes structures near the Moon that display many properties commonly associated with collisionless shocks, including a discontinuity with downstream compression of magnetic field and density, heating and wave activity, and velocity deflections away from the Moon. The two-probe ARTEMIS measurements show that these features do not exist in the pristine solar wind and thus must result from lunar influences. Discontinuity analyses indicate mass flux and heating across the boundary, with the normal velocity dropping from supermagnetosonic to submagnetosonic across the discontinuity. The shock location with respect to crustal magnetic fields suggests a causal relationship, implying that solar wind protons reflected from crustal fields may produce the observed structures. These observations may indicate some of the smallest shocks in the solar system (in terms of plasma scales), driven by solar wind interaction with magnetic fields on the order of the ion gyroradius and inertial length.

1. Introduction and Context

Typically, one thinks of the Moon as an unmagnetized resistive obstacle, which produces a downstream wake by absorbing incident solar wind at the dayside surface, but has little effect outside of the wake, other than the generation of a variety of precursor waves too numerous to list. However, even in the earliest observations of the lunar wake, it became clear that this picture did not always hold. Data from Explorer 35 and Apollo subsatellites indicated that the magnetic fields around the wake, although they showed the expected signature of plasma diamagnetism and rarefaction/recompression, also at times displayed evidence of magnetic compressions outside the wake [*Ness et al.*, 1968; *Colburn et al.*, 1971; *Sonett and Mihalov*, 1972; *Russell and Lichtenstein*, 1975]. It became clear that these resulted from the presence of crustal magnetic fields near the limb, and every subsequent observation has confirmed this association.

However, the precise nature of these features has remained controversial, with some preferring to call them "limb compressions," others "limb shocks," and still others more agnostic terminology. A lack of comprehensive plasma observations hindered discussions, with the best ion data showing compression and a very slight ~3° flow deflection but providing no clear indication of a shock [*Siscoe et al.*, 1969]. As a result, *Russell and Lichtenstein* [1975] stated correctly that "there is no evidence that the plasma is shocked on passage through the features."

More recently, *Lin et al.* [1998] used Lunar Prospector to identify features consistent with the presence of a shock, including electron heating and magnetic turbulence, and a large magnetic amplification at small solar zenith angles and ~100 km altitude, suggesting a standing structure extending upstream from the surface. Statistical studies found numerous similar signatures [*Halekas et al.*, 2006]. However, Lunar Prospector observations left reasonable doubts, since without ion measurements, one could not identify a discontinuity in the flow.

In the last decade, an international fleet of spacecraft has provided a new window on the Moon-plasma interaction. New observations show significant (up to 50% or more) reflection of solar wind protons above crustal magnetic fields [*Futaana et al.*, 2003; *Saito et al.*, 2010; *Lue et al.*, 2011]. Given the sub-gyroradius and sub-inertial-length scale of the lunar fields, one would not expect to see such efficient reflection if protons experienced only magnetic forces. Instead, it appears that electric fields, generated by differential

motion of electrons and ions, help reflect solar wind protons [*Saito et al.*, 2012]. Simulations indicate that these electric fields may form at quite low altitudes [*Deca et al.*, 2014] and that the reflected protons can subsequently interact with the solar wind to drive a compressive interaction with similar properties to that observed by *Fatemi et al.* [2014].

However, the question of "shock" or "compression" remains unanswered, although *Fatemi et al.*'s [2014] results display features consistent with a shock, including compression, heating, and flow deflection. If shocks do exist at the Moon, they may be small, marginal, and/or infrequent, since numerous missions have not found clear evidence for the presence of a shock. In this paper, we report on ARTEMIS observations of phenomena with properties consistent with collisionless shocks, potentially indicating some of the smallest such features in the solar system, at or near the limit of a feature coherent enough to be considered a shock.

2. High-Altitude Observations

ARTEMIS, like previous spacecraft, has observed compressional features at a wide range of altitudes near the limb. In this paper, we discuss two examples with seemingly shock-like properties. We first discuss a lunar flyby by ARTEMIS P2 at moderate altitudes. At this time, ARTEMIS P1 sat just upstream from the Moon, in the undisturbed solar wind. We show a selection of the observations made by the electrostatic analyzer (ESA) [*McFadden et al.*, 2008], fluxgate magnetometer (FGM) [*Auster et al.*, 2008], electric field instrument (EFI) [*Bonnell et al.*, 2008], and search-coil magnetometer (SCM) [*Roux et al.*, 2008] instruments in Figure 1.

As P2 travels past the lunar dusk terminator, from the dayside toward the nightside, it encounters a region of increased plasma wave activity, starting at time "A," seen in the high-frequency electric and magnetic fields, as well as in the low-frequency magnetic field. In addition, we see apparent fluctuations in the electron velocity and temperature onboard moments, much larger than any seen in the preceding undisturbed time period. Intriguingly, the electron velocity fluctuations appear to correlate with the low-frequency magnetic field fluctuations.

We see no change in the ion velocity moments until time "B," when we observe a velocity shift, consisting of a slight slowing and significant deflection of the flow away from the Moon. The electron velocity moments also show similar characteristics, but superimposed upon continuing fluctuations. As the velocity deflection increases, so too does the ion density, the electron temperature, and the magnetic field. The upstream probe, meanwhile, sees no change in the pristine solar wind only a few thousand kilometers away, indicating a localized phenomenon.

In the middle of the ramp, between times "C" and "D," we observe a burst of strong electrostatic and electromagnetic fluctuations, as well as a dip in the magnetic field almost back to pre-event levels. Starting at time B and extending until time "E," we observe an additional ion population at energies below the solar wind. This additional flux peaks between times C and D, at the same time as the features mentioned above, perhaps suggesting an ion-ion instability. After time E, we see an additional ion population at energies above the solar wind.

The peak density, magnetic field, electron temperature, and ion velocity deflection all occur near time E. The density and magnetic field both reach a maximum of a factor of ~2.5 greater than undisturbed values, the electron temperature increases from ~7 to ~10 eV, and the ion velocity deflection reaches ~55 km/s. After time E, disturbed quantities slowly relax back to their undisturbed upstream values, as the spacecraft travels toward the wake. Additional electrostatic fluctuations at the end of the time in Figure 1 may originate in the wake boundary.

The observations discussed thus far display many of the hallmarks of a collisionless shock, including a discontinuity in the flow (greater than the Alfvén velocity of ~45 km/s, on the order of the magnetosonic velocity of 60 km/s), a significant correlated enhancement in the magnetic field and density, and dissipation in the form of electron heating and plasma waves. Also, we observe a low-energy ion population just upstream from and in the ramp, consistent with specularly reflected protons, commonly seen at quasi-perpendicular shocks [*Bale et al.*, 2005]. Downstream, a higher-energy population appears consistent with reflected protons that have subsequently gyrated through the discontinuity. Given the additional ion populations, the distribution is heated in a bulk sense, but ARTEMIS does not resolve the solar wind beam well enough to determine whether that component alone shows evidence of heating.

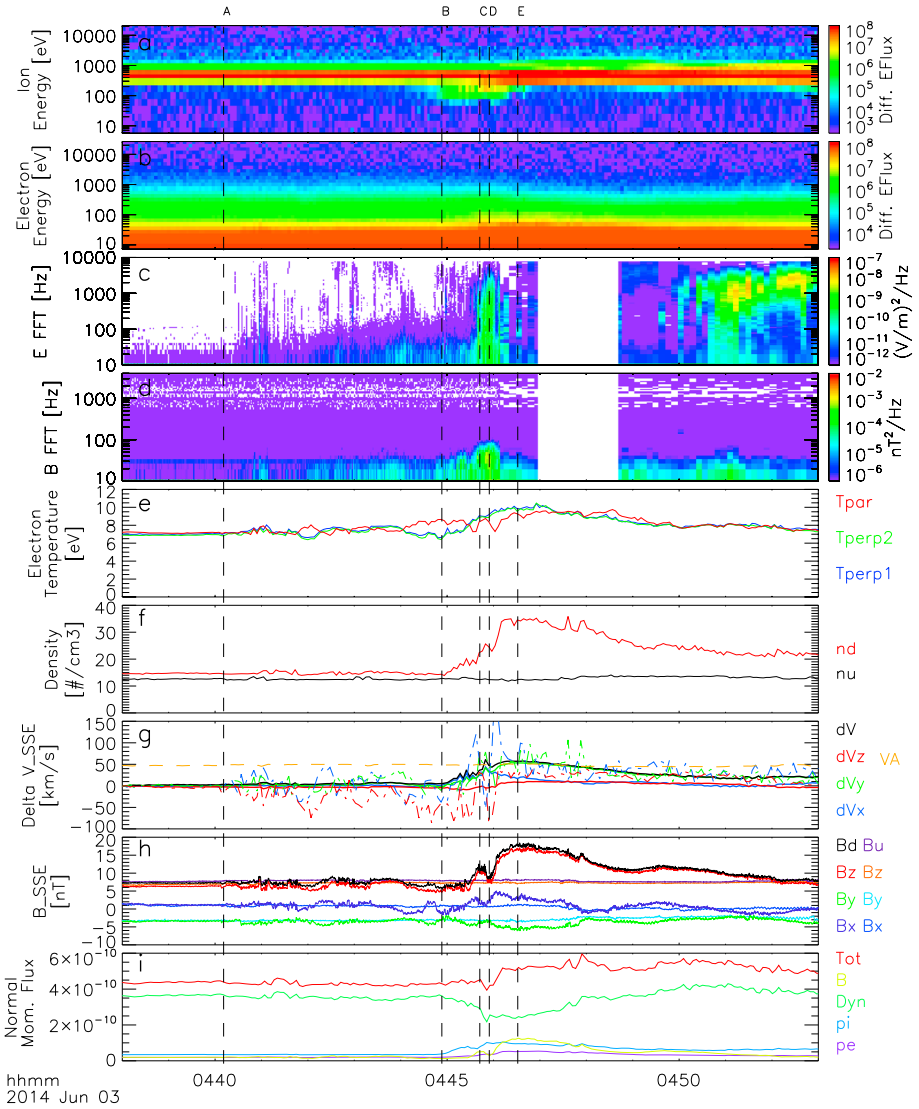

Figure 1. ARTEMIS observations of a lunar flyby (periselene ~420 km) showing (a) ESA measurements of ion energy spectra near the Moon in differential energy flux [eV/(eV cm^2 s sr)]; (b) electron energy spectra in the same units; (c) fast Fourier transforms (FFTs) of electric field fluctuations from EFI; (d) FFTs of magnetic field fluctuations from SCM; (e) onboard electron temperature moments in magnetic field-aligned coordinates; (f) onboard density moments in the undisturbed upstream flow (nu) and near the Moon (nd); (g) change in the ion (solid) and electron (dash-dotted-dash) onboard velocity moments near the Moon, with upstream Alfvén velocity for comparison; (h) magnetic field components and magnitudes measured by FGM in the undisturbed upstream flow (Bu) and near the Moon (Bd); and (i) an illustration of the conservation of momentum flux across the discontinuity, with the orientation derived as described in the text and shown in Figure 2, with electron and ion thermal pressure, normal dynamic pressure, magnetic pressure associated with the component perpendicular to the normal, and the total of the appropriate Rankine–Hugoniot equation (assuming an isotropic plasma). The upstream bulk flow velocity is 300 km/s, the total plasma beta is ~1, the Alfvén Mach number is ~6.5, and the magnetosonic Mach number is ~5. All vectors are in SSE coordinates.

To provide support for the existence of a shock, one should show that the discontinuity satisfies the appropriate Rankine–Hugoniot relations and that there is mass flux across the boundary. We estimate the boundary normal by using the five single-spacecraft methods discussed by *Schwartz* [1998] and taking the average, and show all five normal estimates (which all agree to within 15°), along with the resulting average discontinuity plane, in Figure 2. We then calculate the balance of momentum flux across the boundary (Figure 1i). The result shows enough consistency to support a reasonably accurate determination of the boundary normal, although the small increase across the structure may indicate a slight misalignment. Using this result, we find a normal velocity across the boundary of ~110 km/s on the upstream side and 55 km/s on the

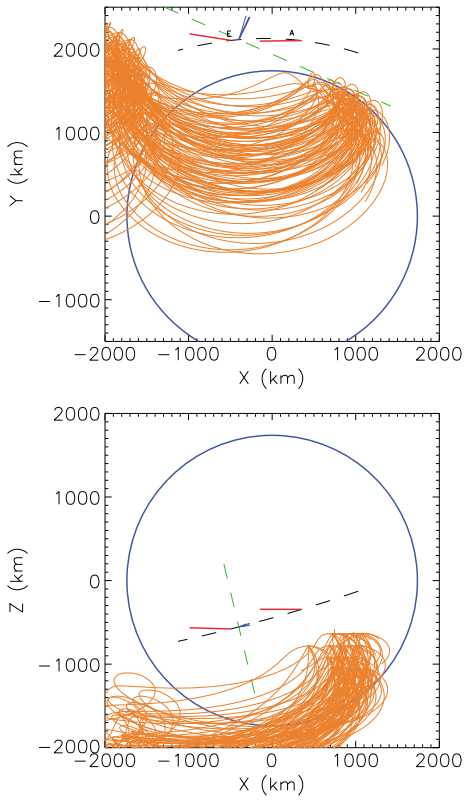

Figure 2. Trajectory of the ARTEMIS probe near the Moon (SSE coordinates) during the time period of Figure 1, in *x-y* and *x-z* projections, with points A and E corresponding to the times marked in Figure 1. The short blue lines show five different methods of approximating the normal to the discontinuity of Figure 1, and the dashed green line shows the boundary corresponding to the average normal. The red lines show the flow velocity vectors upstream and downstream from the discontinuity. The orange curves show inferred trajectories of solar wind protons reflected from the strong group of magnetic anomalies near the limb and upstream from the spacecraft.

downstream side (roughly consistent with the density jump, given the conservation of mass flux across the boundary). Although the bulk flow remains supermagnetosonic, the normal velocity across the discontinuity drops from supermagnetosonic to submagnetosonic, consistent with a shock oriented at a highly oblique angle to the flow (like the Earth's bow shock in the distant tail).

In Figure 2, we also show inferred trajectories of reflected protons from the Moon, assuming reflection from the strong southern farside crustal magnetic fields and tracing reflected protons using undisturbed upstream fields measured by ARTEMIS P1. We note that the strongest crustal magnetic fields sit at a solar zenith angle of about 45°, directly at the upstream extension of the inferred discontinuity. This suggests that solar wind interaction with reflected protons from the Moon could launch the shock-like feature observed by ARTEMIS, consistent with the generation of compressional features seen by *Fatemi et al.* [2014], although they did not claim a shock formed. Figure 2 also suggests that the population of protons seen at the discontinuity by ARTEMIS represents local reflection from the shock rather than a direct measurement of a lunar source, given that inferred trajectories do not reach the spacecraft. Since the convection electric field points into the surface, protons reflected from the Moon cannot easily reach the spacecraft unless the downstream fields significantly differ from the upstream fields.

In fact, the orientation of the convection electric field may prove important for generating the observed features. We note that simulation results [*Fatemi et al.*, 2014] show the greatest solar wind flow deflection and enhancement in density and magnetic field in the hemisphere where the convection electric field points into the surface. In support of this, we have found that most events with shock-like features seen by ARTEMIS occur for a similar geometry (not shown).

We note several unusual features of the observations. First, the electron velocity fluctuations have no obvious origin, although *Scudder et al.* [1986] observed similar features at the Earth's bow shock. If robust, these signatures indicate the existence of significant currents. Second, rather than remaining constant on the downstreamside of the discontinuity, the perturbed parameters quickly return to values close to their upstream values. This may result from the spacecraft entering the wake shortly after passing through the discontinuity and/or from the fact that the interaction must have a rather small lateral scale size and so will decay in amplitude rapidly with downstream distance, as shown by *Fatemi et al.* [2014].

3. Low-Altitude Observations

We now discuss a second ARTEMIS observation, from a more infrequent low-altitude flyby (this time by ARTEMIS P1), reaching a periselene just below 20 km near the dawn terminator. At this time, P2 sat ~10 R_L from the Moon, at large -*Y* monitoring the undisturbed solar wind. We show a similar set of measurements as for the previous example, in Figure 3. The main features of the observation prove similar, but with more significant effects than the high-altitude case.

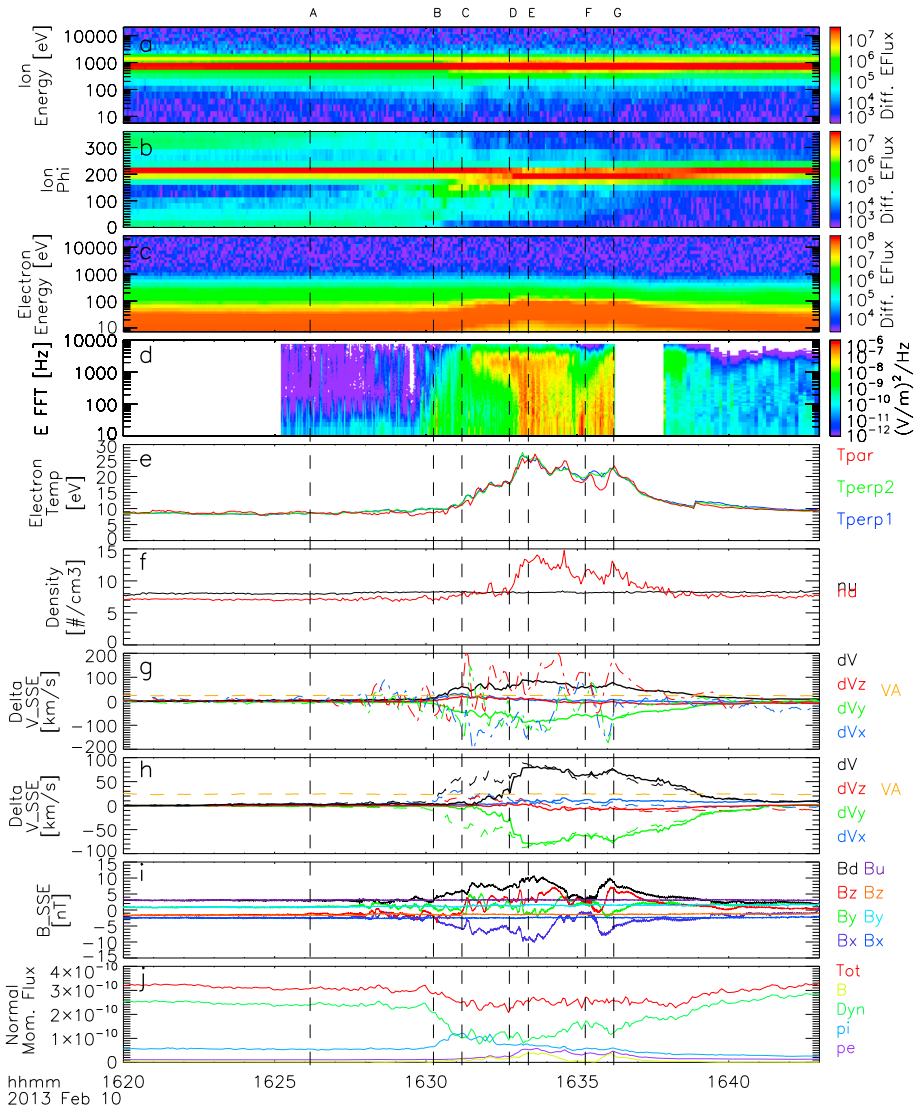

Figure 3. ARTEMIS observations of a lunar flyby (periselene of ~20 km) showing (a) ion energy spectra near the Moon in differential energy flux [eV/(eV cm^2 s sr)]; (b) ion spin-plane angle spectra in the same units; (c) electron energy spectra in the same units; (d) FFTs of electric field fluctuations; (e) onboard electron temperature moments; (f) onboard ion density moments in the undisturbed upstream flow (nu) and near the Moon (nd); (g) change in the ion (solid) and electron (dash-dotted-dash) onboard velocity moments near the Moon, with upstream Alfvén velocity for comparison; (h) change in the ground-computed ion velocity moments for the full distribution (dash-dotted-dash) and partial moments for the solar wind component (solid); (i) magnetic field in the undisturbed upstream flow (Bu) and near the Moon (Bd); and (j) an illustration of the conservation of momentum flux across the discontinuity, in the same format as Figure 1. The upstream bulk flow velocity is 360 km/s, the total plasma beta is ~3, the Alfvén Mach number is ~15, and the magnetosonic Mach number is ~8.

As P1 travels past the lunar terminator, from the dayside toward the nightside, it encounters a diffuse population of reflected protons from the lunar surface [*Saito et al.*, 2008]. This low-level perturbation does not significantly affect the fields seen by ARTEMIS. At time A, we begin to see small fluctuations in the low-frequency magnetic field, and as in the previous case, we observe fluctuations in the electron velocity that appear correlated with the field fluctuations. Between times A and B, these fluctuations increase, and we note the appearance of additional ion populations (most easily seen in the phi spectra of Figure 3b), most likely indicating solar wind reflection from distinct crustal magnetic field sources.

From times B to C, these secondary ion populations become more intense, the magnetic field and the electron temperature begin to increase, and we observe significant deflections in the onboard ion velocity moments, consisting of a slight slowing and significant deflection away from the Moon. The electron velocity

moments show the same trends, but with large fluctuations superimposed. Meanwhile, we see a sharp increase in high-frequency electric field fluctuations.

From times D to E, the ion density jumps by a factor of ~2, the electric field fluctuations increase still further, the electron temperature reaches a factor of ~2.5 greater than ambient, the velocity deflection reaches ~75 km/s, and the magnetic field reaches a factor of ~3 greater than ambient. The upstream solar wind, meanwhile, remains completely steady.

The secondary ion populations prove significant and well separated, and we can calculate separate partial moments for the solar wind and the reflected components of the full 3-D distribution by integrating over selected portions of the distribution. We then calibrate the lower resolution angles obtained from this method by using the higher-resolution onboard moments to ensure that the total velocity moment agrees. This analysis (Figure 3h) shows that most of the initial apparent slowing of the flow, from times B to D, consists of the addition of a new population of ions rather than true slowing of the solar wind. However, the solar wind beam does experience a lateral deflection, reaching a maximum of ~75 km/s, at time E. We note the approximate nature of this value, given the limited phi resolution of the ESA instruments; however, the deflection is readily apparent even in low-resolution distributions available on the ground (see phi spectra of Figure 3b).

After time E, all quantities (especially magnetic field) experience a reduction toward their ambient values, reaching a minimum at time F, before returning to a secondary maximum at time "G." This seeming bifurcation may indicate spatial structure (the magnetic fields at time G are reminiscent in some ways of a flux rope) or temporal changes (i.e., reformation).

As for the higher-altitude example, we estimate the discontinuity normal. Figure 4 shows that the inferred normals do not agree as well as in the previous case (possibly indicating curvature) but at least fall within a 60° cone. Using the boundary thus determined, we calculate the balance of momentum flux across the structure, in Figure 3j, and find a relatively constant value, although the small drop across the structure may indicate a slight misalignment in the inferred normal. The normal velocity drops from 135 km/s to 60 km/s across the structure, consistent with the density jump of a factor of ~2, and indicating significant mass flux across the boundary. The downstream value slightly exceeds the inferred magnetosonic velocity of ~45 km/s, suggesting that we may have slightly overestimated the normal component and/or that the trajectory "skims" the shock surface without reaching the downstream side [*Lin et al.*, 1998].

Once again, the observations display many of the hallmarks of a collisionless shock, including a discontinuity in the flow (significantly greater than the Alfvén velocity of ~25 km/s and greater than the magnetosonic velocity), a significant correlated enhancement in the magnetic field and density, and dissipation in the form of electron heating and plasma waves (more significant at low altitude). Figure 4 provides indications of what may drive this interaction. As seen in Figure 4 (upper right), the main structure peaks just downstream from a reflected ion population with up to ~25% of the incoming solar wind density. This could indicate local reflection at a shock surface or reflection from near the lunar surface. We cannot conclusively differentiate between these possibilities, but note that the velocity vectors of the reflected population appear to emanate directly from a region of strong crustal magnetic field, as shown in Figure 4 (lower right) (crustal field model from *Purucker and Nicholas* [2010]). This region, near the crater Firsov, contains albedo anomalies [*Blewett et al.*, 2011]. These albedo features, typically associated with crustal magnetic fields, may indicate local shielding of the surface from space weathering, suggesting very strong localized reflection of the solar wind.

Despite the strong crustal fields under the spacecraft trajectory, their spatial inhomogeneity ensures that they decay rapidly with altitude, and the predicted field from unmodified crustal sources (Figure 4, bottom right) cannot explain the magnitude of the observed perturbations (Figure 4, bottom left). Thus, ARTEMIS observations suggest an interaction driven by the reflected protons from crustal magnetic fields rather than by the magnetic fields themselves, consistent with *Fatemi et al.* [2014].

4. Implications

The ARTEMIS observations provide strong support for the existence of collisionless shocks at the Moon, but they also leave significant questions. How can we form a shock from an obstacle with a scale size on the

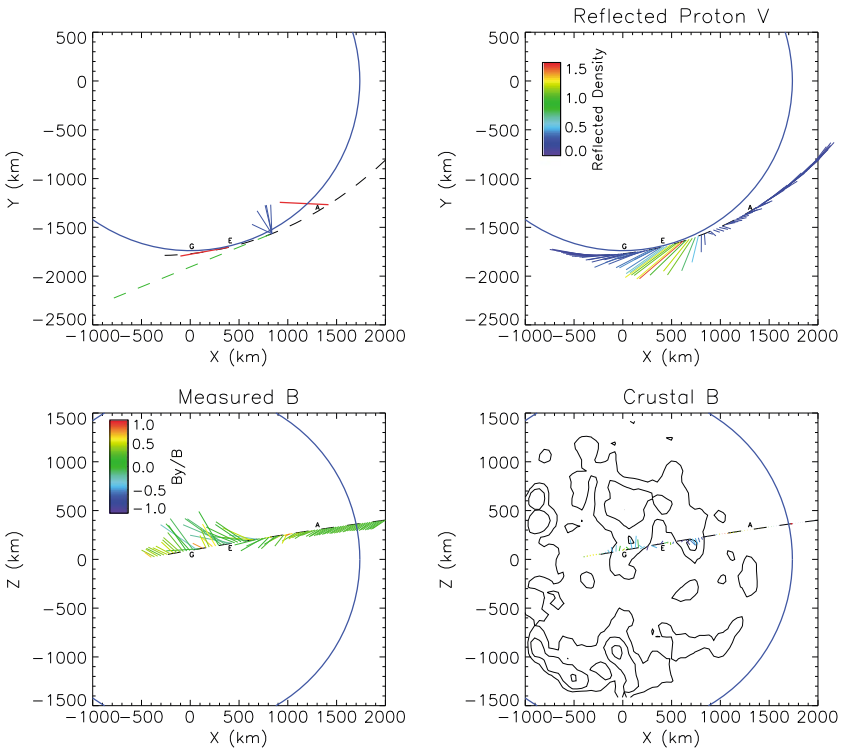

Figure 4. Trajectory of the ARTEMIS probe near the Moon (SSE coordinates) during the time period of Figure 2, with points A, E, and G corresponding to the same times in Figure 3. (upper left) The short blue lines show the five different methods of approximating the normal to the discontinuity of Figure 3, and the dashed green line shows the boundary corresponding to the average normal. The red lines in Figure 4 (upper left) show the flow velocity vectors upstream and downstream from the discontinuity. (upper right) The reflected proton velocity vectors (colored by reflected proton density) derived from ground-computed partial moments. (lower left) The measured magnetic field vectors (colored by out-of-plane component) and (lower right) the expected crustal magnetic field (same length scale, again colored by out-of-plane component) over a contour map of the surface field strength (all from Purucker model). The top two panels show *x-y* projections, while the bottom two show *x-z* projections.

order of or smaller than both the ion gyroradius and inertial length? The answer may lie in the reflected protons, which effectively amplify the effects of the crustal fields. We offer a possible analogy that may help explain the seemingly unreasonable effectiveness of the lunar magnetic fields. Some shocks do not remain stationary but instead constantly "reform," as a result of reflected protons building up to the degree that they can form a new shock [see *Bale et al.*, 2005, and references therein]. These reflected protons also help dissipate energy and lead to well-known shock features such as the "foot" and the "overshoot." *Hada et al.* [2003] performed simulations showing that for typical Mach numbers, on the order of ~20% reflected protons tip the shock into a nonstationary regime. At the Moon, we regularly observe 20% or more reflected protons at low altitudes (*Lue et al.* [2011] report up to 50%). Thus, it seems plausible that if 20% reflected protons cause the formation of a new shock at an already existing shock, a similar percentage of reflected protons from the Moon could produce a new shock entirely. This does not answer the question of how the protons get reflected in the first place, but the low-altitude electric fields implied by Kaguya observations [*Saito et al.*, 2012] and in simulations by *Deca et al.* [2014] and others may explain the initial reflection. Eventually, a full description will have to place the very low altitude proton reflection and the generation of the shock-like structure at several tens of kilometers or higher in a self-consistent framework, but current simulations have difficulty resolving the range of scales to treat the full problem.

The examples shown in this paper represent some of the clearest cases seen by the two ARTEMIS probes in their many hundreds of orbits around the Moon; however, they are by no means the only examples. Although these features, given their minute scale size and highly oblique nature, lie near the margin of what we could presume to call a shock, they still clearly share the relevant properties of larger shocks.

The formation of a shock at the Moon may be a rare event, requiring the optimum orientation of the crustal magnetic fields and the right combination of plasma parameters. However, since we know in advance where these phenomena occur (unlike in interplanetary space), the ARTEMIS observations potentially open up a new regime of shock studies. Further study should help elucidate the necessary conditions for the formation of shocks at the smallest possible scales, with a corresponding gain in our understanding of shock physics in other contexts.

Acknowledgments

We thank the Solar System Exploration Research Virtual Institute for supporting this study (SSERVI-2014-225). We acknowledge NASA contract NAS5-02099 for the use of ARTEMIS data and specifically J.W. Bonnell and F.S. Mozer for the EFI data and A. Roux and O. LeContel for the SCM data. All ARTEMIS data are publicly available at http://artemis.ssl.berkeley.edu and NASA's CDAWeb. K.H.G. was financially supported through the German Ministry for Economy and Energy and the German Center for Aviation and Space (DLR) under contract 50 OC 1001.

The Editor thanks Zdenek Nemecek and an anonymous reviewer for their assistance in evaluating this paper.

References

Auster, H. U., et al. (2008), The THEMIS fluxgate magnetometer, *Space Sci. Rev.*, *141*, 235–264.

Bale, S. D., et al. (2005), Quasi-perpendicular shock structure and processes, *Space Sci. Rev.*, *118*, 161–203.

Blewett, D. T., E. I. Coman, B. R. Hawke, J. J. Gillis-Davis, M. E. Purucker, and C. G. Hughes (2011), Lunar swirls: Examining crustal magnetic anomalies and space weathering trends, *J. Geophys. Res.*, *116*, E02002, doi:10.1029/2010JE003656.

Bonnell, J. W., F. S. Mozer, G. T. Delory, A. J. Hull, R. E. Ergun, C. M. Cully, V. Angelopoulos, and P. R. Harvey (2008), The electric field instrument (EFI) for THEMIS, *Space Sci. Rev.*, *141*, 303–341.

Colburn, D. S., J. D. Mihalov, and C. P. Sonett (1971), Magnetic observations of the lunar cavity, *J. Geophys. Res.*, *76*, 2940–2957, doi:10.1029/JA076i013p02940.

Deca, J., A. Divin, G. Lapenta, B. Lembège, S. Markidis, and M. Horányi (2014), Electromagnetic particle-in-cell simulations of the solar wind interaction with lunar magnetic anomalies, *Phys. Rev. Lett.*, doi:10.11103/PhysRevLett.112.151102.

Fatemi, S., M. Holmström, Y. Futaana, C. Lue, M. R. Collier, S. Barabash, and G. Stenberg (2014), Effects of protons reflected by lunar crustal magnetic fields on the global lunar plasma environment, *J. Geophys. Res. Space Physics*, *119*, 6095–6105, doi:10.1002/2014JA019900.

Futaana, Y., S. Machida, Y. Saito, A. Matsuoka, and H. Hayawaka (2003), Moon-related nonthermal ions observed by Nozomi: Species, sources, and generation mechanisms, *J. Geophys. Res.*, *108*(A1), 1025, doi:10.1029/2002JA009366.

Hada, T., M. Oonishi, B. Lembège, and P. Savoini (2003), Shock front nonstationarity of supercritical perpendicular shocks, *J. Geophys. Res.*, *108*(A6), 1233, doi:10.1029/2002JA009339.

Halekas, J. S., D. A. Brain, D. L. Mitchell, R. P. Lin, and L. Harrison (2006), On the occurrence of magnetic enhancements caused by solar wind interaction with lunar crustal fields, *Geophys. Res. Lett.*, *33*, L01201, doi:10.1029/2006GL025931.

Lin, R. P., D. L. Mitchell, D. W. Curtis, K. A. Anderson, C. W. Carlson, J. McFadden, M. H. Acuña, L. L. Hood, and A. B. Binder (1998), Lunar surface magnetic fields and their interaction with the solar wind: Results from Lunar Prospector, *Science*, *281*, 1480–1484.

Lue, C., Y. Futaana, S. Barabash, M. Wieser, M. Holmström, A. Bhardwaj, M. B. Dhanya, and P. Wurz (2011), Strong influence of lunar crustal fields on the solar wind flow, *Geophys. Res. Lett.*, *38*, L03202, doi:10.1029/2010GL046215.

McFadden, J. P., C. W. Carlson, D. Larson, M. Ludlam, R. Abiad, B. Elliott, P. Turin, M. Marckwordt, and V. Angelopoulos (2008), The THEMIS ESA plasma instrument and in-flight calibration, *Space Sci. Rev.*, *141*, 277–302.

Ness, N. F., K. W. Behannon, H. E. Taylor, and Y. C. Whang (1968), Perturbations of the interplanetary magnetic field by the lunar wake, *J. Geophys. Res.*, *73*, 3421–3440, doi:10.1029/JA073i011p03421.

Purucker, M. E., and J. B. Nicholas (2010), Global spherical harmonic models of the internal magnetic field of the Moon based on sequential and coestimation approaches, *J. Geophys. Res.*, *115*, E12007, doi:10.1029/2010JE003650.

Roux, A., O. le Contel, C. Coillot, A. Bouabdellah, B. de la Porte, D. Alison, S. Ruocco, and M. C. Vassal (2008), The search coil magnetometer for THEMIS, *Space Sci. Rev.*, *141*, 265–275.

Russell, C. T., and B. R. Lichtenstein (1975), On the source of lunar limb compression, *J. Geophys. Res.*, *80*, 4700, doi:10.1029/JA080i034p04700.

Saito, Y., et al. (2008), Solar wind proton reflection at the lunar surface: Low energy ion measurements by MAP-PACE onboard SELENE (KAGUYA), *Geophys. Res. Lett.*, *35*, L24205, doi:10.1029/2008GL036077.

Saito, Y., et al. (2010), Inflight performance and initial results of Plasma energy Angle and Composition Experiment (PACE) on SELENE (Kaguya), *Space Sci. Rev.*, *154*, 265.

Saito, Y., M. N. Nishino, M. Fujimoto, T. Yamamoto, S. Yokota, H. Tsunakawa, H. Shibuya, M. Matsushima, H. Shimizu, and F. Takahashi (2012), Simultaneous observation of the electron acceleration and ion deceleration over lunar magnetic anomalies, *Earth Planets Space*, *64*, 83–92.

Schwartz, S. J. (1998), Shock and discontinuity normal, Mach numbers, and related parameters, in *Analysis Methods for Multi-Spacecraft Data*, edited by G. Paschmann and P. W. Daly, ISSI Sci. Rep. SR-001, ESA Publications Division, Noordwijk, Netherlands.

Scudder, J. D., A. Mangeney, C. Lacombe, C. C. Harvey, T. L. Aggson, R. R. Anderson, J. T. Gosling, G. Paschmann, and C. T. Russell (1986), The resolved layer of a collisionless, high β, supercritical, quasi-perpendicular shock wave 1. Rankine-Hugoniot geometry, currents, and stationarity, *J. Geophys. Res.*, *91*, 11,019–11,052, doi:10.1029/JA091iA10p11019.

Siscoe, G. L., E. F. Lyon, J. H. Binsach, and H. S. Bridge (1969), Experimental evidence for a detached lunar compression wave, *J. Geophys. Res.*, *74*, 59–69, doi:10.1029/JA074i001p00059.

Sonett, C. P., and J. D. Mihalov (1972), Lunar fossil magnetism and perturbations of the solar wind, *J. Geophys. Res.*, *77*, 588–603, doi:10.1029/JA077i004p00588.